Journal of Applied Polymer Science

Molecular Modeling Approach to the Prediction of Mechanical Properties of Silica-Reinforced Rubbers

Reinhard Hentschke,[1] Jonathan Hager,[1] Nils W. Hojdis[2]

[1]Fachbereich Mathematik und Naturwissenschaften, Bergische Universität, Wuppertal, North Rhine-Westphalia D-42097, Germany

[2]Continental Reifen Deutschland GmbH, Hanover, Lower Saxony D-30419, Germany

Correspondence to: R. Hentschke (E-mail: hentschk@uni-wuppertal.de)

ABSTRACT: Recently, we have suggested a nanomechanical model for dissipative loss in filled elastomer networks in the context of the Payne effect. The mechanism is based on a total interfiller particle force exhibiting an intermittent loop, due to the combination of short-range repulsion and dispersion forces with a long-range elastic attraction. The sum of these forces leads, under external strain, to a spontaneous instability of "bonds" between the aggregates in a filler network and attendant energy dissipation. Here, we use molecular dynamics simulations to obtain chemically realistic forces between surface modified silica particles. The latter are combined with the above model to estimate the loss modulus and the low strain storage modulus in elastomers containing the aforementioned filler-compatibilizer systems. The model is compared to experimental dynamic moduli of silica filled rubbers. We find good agreement between the model predictions and the experiments as function of the compatibilizer's molecular structure and its bulk concentration. © 2014 Wiley Periodicals, Inc. J. Appl. Polym. Sci. **2014**, *131*, 40806.

KEYWORDS: elastomers; mechanical properties; rubber; supramolecular structures; theory and modeling

Received 20 December 2013; accepted 31 March 2014

DOI: 10.1002/app.40806

INTRODUCTION

Dynamic moduli in terms of amplitude, frequency, or temperature are essential for the developer of filled rubber applications. In this context, the advent of silanized silica as filler material in automobile tire treads (1992, introduction of the green tire[1] brought about significant increase in compound variability due to the compatibilizer chemistry. In addition to size, shape, and morphology of the filler and various chemically as well as physically different types of rubbers, there now exists a vast number of chemical and physical variations that may be introduced through the compatibilizing agents. This affects the macroscopic performance parameters like rolling resistance, wet grip, tread wear etc.[2–4] Consequently, it is highly desirable to develop theoretical approaches allowing the prediction of molecular ingredients for rubber compounds with specifically improved macroscopic performance.

An effect of major importance in this context was extensively studied in the 1960s by A. R. Payne. The effect, already observed by a number of researchers in the early 1940s,[5] now bears his name (an early review is Ref. 6; more recent reviews are Refs. 7–9). The Payne effect describes the marked decrease of the storage modulus, μ', with increasing strain amplitude, u_o, in filled rubbers under cyclic loading. Because the effect does not occur in unfilled rubbers, its cause must be related to either the rubber-filler or the filler-filler interface(s). Various explanations and models have been suggested to explain and to quantitatively describe/predict the Payne effect, including filler network breakdown[6,10] (chapter 3)[11–13] filler deagglomeration,[14,15] polymer debonding from filler surface,[16,17] strain softening of the polymer shell surrounding fillers,[18] or micromechanical approaches.[7,8] Nevertheless, it is fair to say that still there are different scenarios on the molecular scale discussed controversially. In particular, it is not yet possible to theoretically predict dynamic moduli based solely on the knowledge of molecular ingredients in a rubber compound or their molecular interactions.

Recently, we have suggested a nanomechanical model for dissipative loss in filled elastomer networks in the context of the Payne effect.[19] The mechanism is based on the sum of molecular forces leading to a loop in the stress-strain relation, which gives rise to spontaneous displacements between filler particles on the nanometer scale. In this work, we use molecular dynamics (MD) simulations to obtain the microscopic interactions forces between compatibilizer covered silica particles. These force curves are combined with the above model to estimate both the loss modulus, μ'', and the low strain storage modulus, μ', associated with the filler network, in elastomers containing the aforementioned filler-compatibilizer systems. We find good

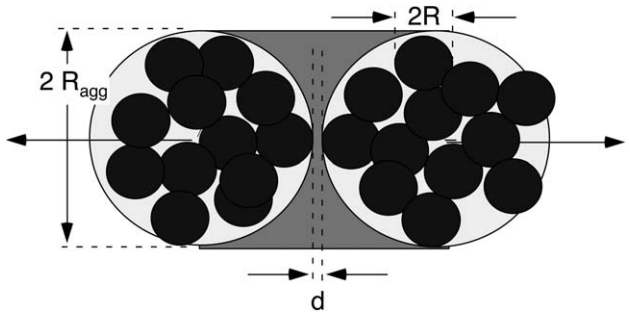

Figure 1. Two aggregates possessing a single direct contact between two primary particles (black circles) separated by the distance d. The dark shaded area is a rubber bridge linking the aforementioned aggregates represented by effective spheres of radius R_{agg}. Horizontal arrows indicate external forces acting on the two aggregates.

agreement between the predictions of our model and the experimental moduli as function of compatibilizer size and surface concentration.

NANOMECHANICAL MODEL FOR DISSIPATIVE LOSS IN FILLER NETWORKS

Filled rubbers acquire most of their mechanical strength through fillers forming spanning branched networks throughout the rubber matrix. Transmission electron micrographs (TEM) (a number of nice examples can be found in Ref. 10; more recent examples are, for instance, Figure 7.3 in Ref. 9 or Figure 3.8 in Ref. 20) usually show filler network structures based on connected fractal filler "flocs" build of agglomerates, which in turn consist of small aggregates composed of primary filler particles. The aggregates are considered as "unbreakable." Their superstructures however are stabilized by comparatively weak bulk dispersion and interface forces. This picture is supported by the pronounced dependence of the (low strain) storage modulus, μ', on filler volume fraction, ϕ, in the form of a power law, $\Delta\mu'(u_o) \sim \phi^y$, where y can be as high as 3.5 or even higher as shown in Ref. 21. Here, u_o is the dynamic strain amplitude, and Δ indicates that μ' is calculated relative to a base value, which encompasses contributions from other sources not described by the power law. These sources are the pure elastomer network, the so-called hydrodynamic effect, whose by comparison weak dependence on ϕ is neglected here, as well as a contribution due to filler-rubber interaction, which also is independent of the strain amplitude to good approximation. In practice, $\Delta\mu'(u_o) = \mu'(u_o) - \mu'(\infty)$, where ∞ is around 100% strain. For a detailed discussion see Refs. 9 and 22.

The following is a summary of the model originally suggested and discussed in Ref. 19. We focus on one such "breakable" aggregate-to-aggregate contact within a branch formed by aggregates in the aforementioned filler network. Suppose that two aggregates along the branch, as shown in Figure 1, do interact via the following forces,

$$f = f_{pp} + f_{matrix}, \quad (1)$$

schematically depicted in the top panel of Figure 2. Here, f_{pp} is the force between two adjacent primary particles, each belonging to a different aggregate. Of course, there may be more than one direct contact between two aggregates, and we return to this point below. The solid line in Figure 2 shows that we may expect a loop in the resultant aggregate-aggregate interaction, that is, the sum of short-range repulsion, dispersion attraction, and the rubber bridge's response to deformation.

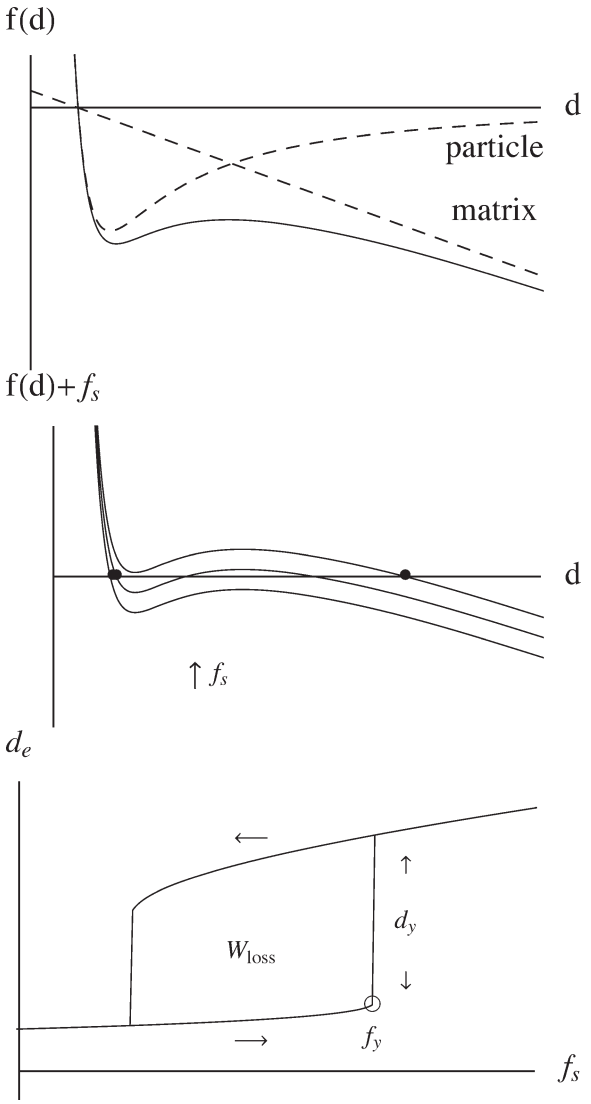

Figure 2. (top) Cartoon of the force-distance relation, f versus d, pertaining to a breakable aggregate-aggregate contact. Here, "particle" refers to the direct interaction force, f_{pp}, between two filler primary particles possibly including coupling agents at their surfaces. "Matrix" refers to the elastic deformation force, f_{matrix}, of the rubber bridge in the previous figure. The solid line is the net force due to the aforementioned contributions. (middle) The d-independent external force f_s causes a vertical displacement of the previous net force f, shifting the force equilibrium to larger d values, d_e (indicated by the solid circles). (bottom) Hysteresis in the $f_s - d_e$-plane. The quantities W_{loss} and f_y are the dissipated energy per one cycle and the yield force at which the spontaneous displacement d_y occurs during extension.

The consequences of this force function are explored in the middle panel of Figure 2. The three force curves correspond to different values of a constant force, f_s, in addition to f. Here, constant means that f_s does not depend on the interparticle

separation, d, introduced in Figure 1. The force f_s arises as follows. The (cyclic) external stress, acting on a sample of the rubber material, is mainly transmitted along its filler network branches. In particular, it is transmitted through filler contacts of which Figure 1 is a pictorial example. Our f_s, which may be positive (extension of the contact) or negative (compression of the contact), is an effective average force normal to the contact as a result of the externally applied stress. Due to the assumed orientational average over all contacts in the sample, however, there is no specific relation between the sign of f_s in this model and the signs of external stress components at any particular time. In the following, we assume local equilibrium, that is, even though f_s is the consequence of a dynamic force on the macroscopic scale, on the microscopic level of the aggregates the sum of the aforementioned forces is zero. Thus, f_s causes the vertical displacement of f and, if f_s is positive, shifts the equilibrium interparticle separation, d_e, continuously to the right. When the local minimum of the aforementioned force loop crosses the x-axis, then d_e"jumps" spontaneously to a distinctly larger value. Further increase of f_s again results in a continuous increase of d_e. The subsequent decrease of f_s leads to hysteresis, because there is a "jump-in" when the local maximum of the force loop crosses the x-axis from above. The attendant path in the f_s-d_e-plane is shown in bottom panel of Figure 2. The area enclosed by the two curves, W_{loss}, is the energy dissipated along the indicated path. The circle marks the yield force, f_y, at which the jump on extension occurs.

In our previous discussion of the model in Ref. 19, we had studied the dependence of W_{loss} and f_y on the parameters of a simple model for f. The dispersion attraction was modeled in terms of Hamaker forces between primary particles. What we mean by Hamaker force is the weak attractive force between electrically neutral bodies, which for two spheres with the same radius R and closest surface-to-surface separation d, has the form, $-A\ R/12\ d^2$. The Hamaker constant A, on the simplest level, is calculated by pairwise summation over the atomic dispersion interactions across the spheres.[23] In addition, we had considered aggregates consisting of one primary particle only. Even though this is unrealistic for quantitative predictions, the qualitative aspects remain valid. Here, we present a more realistic calculation, that is, the force f_{pp} is obtained via MD simulations of compatibilizer covered crystalline surfaces of SiO_2. Before returning to discuss details of the MD, we briefly explain how the MD is used to obtain f_{pp}.

The result of our MD simulations is the average potential interaction energy between the surfaces, $U(D)$, shown in the example in Figure 3 as function of their separation D. From the negative derivative with respect to D , we obtain the force $f_{cryst}(D)$ (in units of nN/nm^2). This force is converted to $f_{pp}(d)$, the corresponding force between two spheres of radius R and closest surface-to-surface distance d, via

$$f_{pp}(d) = \int_0^{\pi/2} dA(\theta) \cos\theta\ f_{cryst}(D), \qquad (2)$$

where $dA(\theta) = 2\ \pi\ R^2\ \sin\theta d\theta$ and $D = d + 2\ R\ (1 - \cos\theta)$. The notation is explained in Figure 5. An example for $f_{pp}(d)$ is

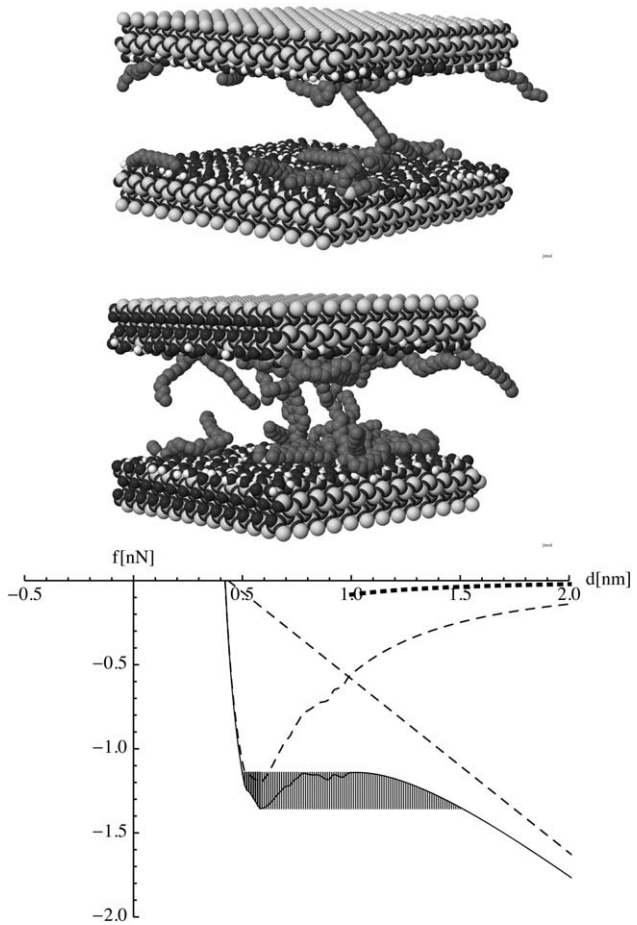

Figure 3. MD snapshots of two slaps of β-cristobalite (100) covered with a compatibilizer (AS216; the notation is explained in Figure 4) at $T = 300$ K. Periodic boundary conditions are applied parallel to the surfaces. The compatibilizer surface number densities in these examples are $0.156\ nm^{-2}$ (top) and $0.416\ nm^{-2}$ (middle). (bottom) Curved dashed line: MD result for the system in the top panel after conversion to f_{pp} via eq. (2) using $R = 15$ nm; straight dashed line: f_{matrix} using the rubber shear modulus $\mu = 0.5$ MPa; solid line: sum of the dashed force curves; thick dotted line: Hamaker force, $-A\ R/12\ d^2$, using the Hamaker constant $A = 40$ kJ/mol for fused silica taken from Ref. 23. The shaded area is W_{loss}.

shown in the bottom panel of Figure 3. We emphasize that already Payne[24] had discussed Hamaker forces between the filler particles as possible reason for the compounds stability (based on earlier work of van den Tempel[25]. In fact, the break up of the network under strain then would give rise to the decrease of the storage modulus. The idea was criticized, because Hamaker interparticle forces were considered as too weak (cf. Ref. 7). The Hamaker interaction included in Figure 3 (bottom panel) is for "naked" silica and will be significantly reduced by the compatibilizer layer between the silica surfaces. In the following, we do not include the Hamaker force, but a more refined calculation should include this interaction as well.

During a MD simulation, the classical equations of motion of atoms in a simulation volume are solved numerically.[26] The forces between atoms are derived from empirical potential energy functions (Ref. 27). The present simulations build upon the Universal Force Field (UFF) potential energy function introduced in

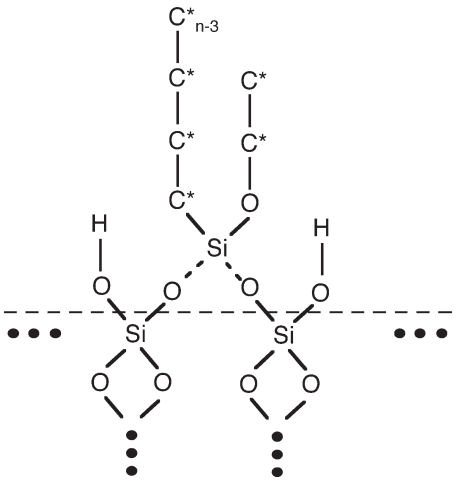

Figure 4. Illustration of the compatibilizer (AS2n) coupling to the silica surface. Stars indicate united atom carbon atoms. Vertical rows of dots indicate the bulk silica atoms, for which the partial charges are taken to be zero. The same applies to the united atoms labeled $(n-3)$, where $(n-3)$ is the number of united atom carbons in this alkyl moiety (in this study $n = 3$, 8, and 16). The other partial charges were computed as specified in the text. Horizontal rows of dots indicate the repeated occurrence of the unit shown in the center either with the compatibilizer attached (dashed bonds) or hydroxyl groups instead depending on compatibilizer surface coverage.

Ref. 28, including a parameterization adapted to the present system. The only coarse-graining applied here is that hydrogen atoms bonded to carbon atoms are fused with the latter to form united atoms. Our systems (cf. above) consist of two parallel slaps cut from a β-cristobalite (100) surface. This is because the silanol group density on this crystalline silica surface closely corresponds to what is found in the case of industrial amorphous silica. Compatibilizer molecules are "planted" randomly on the slab surfaces until the desired surface density is reached. The atoms below the dashed horizontal line in Figure 4 are kept at fixed positions relative to each other. All other atoms are mobile. The bonding of the compatibilizer molecules to the surface follows the model put forward by Deschler et al.[29] (cf. Figure 4). Compatibilizer partial charges are calculated on the Möller-Plesset (MP2) level in conjunction with the electrostatic potential fitting algorithm using Spartan 08 (Version 1.0).[30] The surface charges of β-cristobalite are taken from Ref. 31. Periodic boundary conditions are applied parallel to the surfaces. Subsequently, the potential energy of interaction between the two slab surfaces is calculated for variable D, the surface-to-surface separation, as the slab surfaces are moved (rate: 1 Å/100 pS) toward each other. This procedure is repeated 10 times, and $U(D)$ is the average for each value of D obtained from these independent runs. The negative gradient then yields the force curves as explained above. All simulations are carried out at room temperature (300 K).

The rubber matrix is included as a continuous linear elastic "collar" surrounding the contact, cf. the shaded area in Figure 1, that is,

$$f_{\mathrm{matrix}} \propto -(d-d_{\mathrm{o}}). \tag{3}$$

In principle, d_{o} is the equilibrium interparticle separation when all other particle-particle interactions are omitted. However, in all concrete calculations, we set d_{o} equal to the zero of $f_{\mathrm{pp}}(d)$ (cf. the upper panel in Figure 2). The specific form of f_{matrix} is approximated based on the simple linear stress-strain relationship $df_{\mathrm{matrix}}(\Theta)/(\cos\Theta dA(\Theta))=3\mu\Delta/l(\Theta)$. Here, μ is the shear modulus of the (unfilled) rubber. In addition, $l(\Theta)=d_{\mathrm{o}}+2R_{\mathrm{agg}}(1-\cos\Theta)$ and $dA(\Theta)=2\pi R_{\mathrm{agg}}^2\sin\Theta d\Theta$. The quantity $l(\theta)$ is the closest surface-to-surface separation between two spheres of the same radius R_{agg} along a set of lines, defined through the angle θ, each of which is parallel to the line connecting the sphere's centers. $dA(\theta)$ is the attendant circular surface element (cf. Figure 5). This notation again is explained in Figure 5. The total force, $\int_0^{\pi/2} df_{\mathrm{matrix}}(\Theta)$, is given by

$$f_{\mathrm{matrix}} \approx 6\pi\mu R_{\mathrm{agg}} \left(\coth^{-1}(1+\frac{d_{\mathrm{o}}}{R_{\mathrm{agg}}})-\frac{1}{2}\right)\Delta \tag{4}$$

$(R \gg d_o)$. f_{matrix} is the force necessary to displace a sphere of radius R_{agg} by the distance $\Delta=d-d_{\mathrm{o}}$ in the setup shown in Figure 1. This expression is similar to the exact expression $6\pi\mu R\Delta$, the force needed to displace a macroscopic sphere of radius R embedded in a rubber matrix with shear modulus μ by a small distance Δ.[32] Notice that $\coth^{-1}(1+x)-1/2 \approx 2$ if $x=0.01$ and ≈ 1 if $x=0.1$, which covers the relevant range of d_o/R_{agg}-values.

EXPERIMENTAL

Materials

The rubber is a blend of natural rubber (NR) and styrene-butadiene rubber (SBR) with 25% styrene and 50% vinyl content. The silica

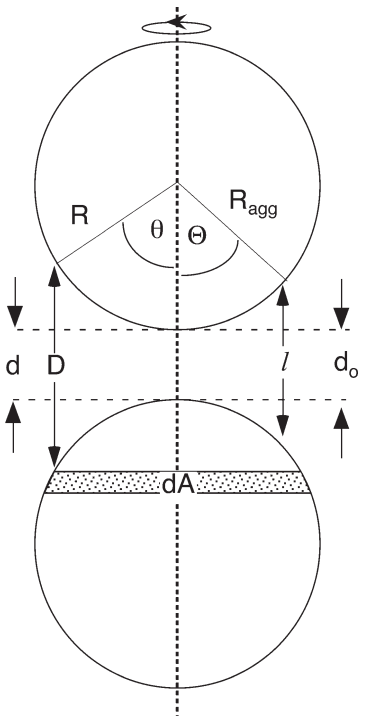

Figure 5. Notation used in eq. (2) (to the left of the vertical dashed lines) and in eq. (3) (to the right of the vertical dashed line). Notice that in this drawing the radii R and R_{agg} are identical solely for reason of convenience.

Table I. Formulation Used

Compounds	Ratio (phr)
NR	20
SBR (25/50)	80
Silica	95
Mineral oil	35
ZnO	2.5
Antiaging agents	4.0
Stearic acid	2.5
Compatibilizer	Variable

used here has a specific cethyltrimethylammoniumbromide (CTAB) surface area of approximately 160 m^2/g and a specific Brunauer-Emmet-Teller (BET) surface area of approximately 175 m^2/g. Triethoxypropylsilane and triethoxyoctylsilane were used as compatibilizers. Materials and their amounts in units of phr (parts per hundred rubber) are listed in Table I. In order to focus on the interaction between filler particles or aggregates, no vulcanization chemicals are part of the formulation.

Preparation of Specimens

The internal kneader was a Werner und Pfleiderer Typ GK 1,5 E with intermeshing rotor geometry. The compound was mixed 7 min with a drop temperature of 150°C so that the reaction of the compatibilizer and the silica has taken place.

Dynamic-Mechanical Characterization

The dynamic-mechanical characterization of the mixed rubber samples was done on a Rubber Process Analyzer from Alpha Technologies as a strain amplitude dependent measurement. All samples were conditioned via a full strain sweep from 0.3% to 100% in shear at a temperature of 70°C with a frequency of 1 Hz. The experimental data discussed below were taken during the second strain sweep under identical conditions.

COMPARISON TO EXPERIMENTAL DATA

From our model based on a single aggregate-to-aggregate interaction, we can estimate albeit roughly, the storage and the loss modulus as functions of strain amplitude. First, we observe that the yield force, where the jump occurs, is directly related to the compound strength as measured by $\Delta\mu'$ at low strain, $\Delta\mu'(0)$, that is,

$$\Delta\mu'(0) \propto f_y \ . \tag{5}$$

Notice that the initial modulus, here we mean the contribution to the storage modulus in the small strain limit due to the contacts between aggregates, is proportional to the applied force divided by the attendant displacement. In other words, it is proportional to the derivative of the force curve, for example, the solid line in the bottom panel of Figure 3, with respect to d close to equilibrium. This derivative can be either determined directly from the force curve. Or, and this is done here, it may be estimated via f_y divided by the attendant surface-to-surface displacement, that is, the displacement from where the force is zero to where the contact yields to strain. Because the latter displacement varies much less than f_y, we may use the yield force as a measure for the contact's stiffness. Thus, we arrive at the above approximate relation. Below, we apply relation (5) to measurements of the storage modulus as function of compatibilizer surface density. Thus, we may determine the proportionality constant from one experimental concentration and use the same constant for all others. We emphasize that our theory is not a statistical theory, that is, does not predict the average fraction of closed contacts. Thus, our prediction of the storage modulus as well as our prediction of the loss modulus below are limited to strain amplitudes for which this fraction can be estimated by simple means.

Second, we use the formula $w=\pi\mu'' u_o^2$ to estimate the loss modulus (e.g., Ref. 33). Notice that the quantity w is the dissipated energy density during one period of a sinusoidal cyclic strain with an amplitude u_o, $u=u_o\sin(\omega t+\delta)$, and a likewise sinusoidal response, $\sigma=\sigma_o\sin(\omega t)$, that is, $w=\oint\sigma du=\int_0^{2\pi/\omega}\sigma\dot{u}dt$. Using $\mu'=(\sigma_o/u_o)\cos\delta$ and $\mu''=(\sigma_o/u_o)\sin\delta$ yields the above equation relating w to μ''. Thus, $w=(W_{\mathrm{loss}}/N_A)(\kappa\phi/V_{\mathrm{agg}})$ or

$$\mu''=(W_{\mathrm{loss}}/N_A)(\kappa\phi/V_{\mathrm{agg}}\pi u_o^2). \tag{6}$$

The quantity N_A is Avogadro's constant, ϕ is the filler volume fraction, and $V_{\mathrm{agg}}=4\pi R_{\mathrm{agg}}^3/3$ is the aggregate volume. Here, W_{loss} is the dissipated energy per contact during one cycle as depicted in Figure 2 in units of Joule per mol. Notice that ϕ/V_{agg} is the number density of aggregates in the sample and κ is the average number of broken contacts per aggregate.

The quantity κ is difficult to determine. In particular, we do not know its dependence on u_o. Here, we assume $u_o \approx 0.1$, because it narrows κ to a reasonable range using the following rational argument: we may assume that almost all, that is, 80%–90%, of the filler-filler contacts responsible for the Payne effect, are broken at this amplitude. This is based on the phenomenological models proposed by Kraus[11] and subsequently by Maier and Göritz.[16] The models describe the functional form of the Payne effect as well as that of the attendant loss modulus (a summary is presented in Chapter 7 of Ref. 9). They may be fitted to existing experimental data, and, because one fit parameter is the ratio of broken to unbroken contacts, we are able to deduce the quoted percentages. Larger u_o are less useful, because the experimental loss modulus becomes small and its magnitude is strongly affected by the polymer network, whose energy dissipation is not included in the current model, as well as by experimental scatter. In addition it is reasonable to assume that the maximum value for κ is about 3, because three contacts between rigid bodies do fix their respective positions and orientations. Thus we conclude that $\kappa(u_o \approx 0.1)$ is between 1 and 3, ignoring branch points of the filler network possessing larger κ values.

In the following, we use a primary particle radius $R=15$ nm, which is rather typical for commercial rubber applications. Nevertheless, in reality, R as well as the aggregate size, R_{agg}, do have broad distributions (e.g., Ref. 34). Our value of $R_{\mathrm{agg}}=50$

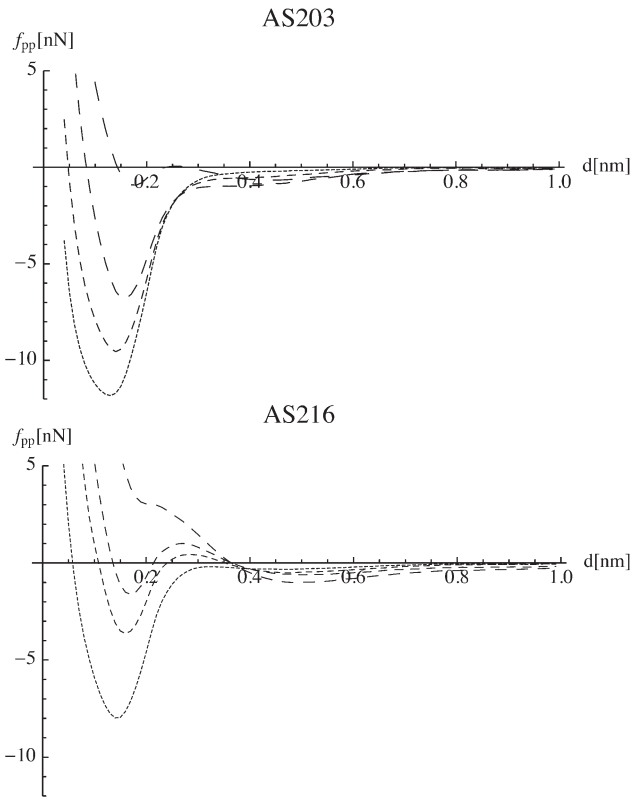

Figure 6. Forces f_{pp} versus d obtained via MD and conversion to spherical particles according to eq. (2). (top) Length of dashes increases with increasing surface density. Densities included are 0.017, 0.52, 0.121, and 0.21 compatibilizers/nm^2. (bottom) Length of dashes increases with increasing surface density (0.017, 0.039, 0.052, and 0.087 compatibilizers /nm^2).

nm is based on the recent TEM and Small Angle X-ray Scattering study in Ref. 34.

Before we discuss our own data we take a look at Ref. 35. The authors discuss the influence of silanization on dynamic-mechanical properties of silica in Nitrile Rubber/Butadiene Rubber (NBR/BR) blends. Without silane coating their $\mu''(10\%)$ is between 0.95 and 1.15 MPa for the two different formulations at room temperature, where we have subtracted 0.1 MPa for the matrix (cf. their Figure 7). The filler content is about $\phi=0.15$. Using $\mu=0.5$ MPa also inferred from their data, we obtain, based on the lowest force curve (dotted line) in the top panel of Figure 6 and using eq. (6), $0.4\,\text{MPa} < \mu''(10\%) < 1.2\,\text{MPa}$ for $1 \leq \kappa \leq 3$. Thus, considered the complexity of the system, the result appears reasonable. The displacement d_y in this particular case is 7.5 nm.

Before we apply relation (5) and the approximation (6) to our own experimental data, we discuss the latter themselves. Figure 7 shows the experimental storage modulus, μ', and the experimental loss modulus, μ'', at the respective strain amplitudes of 0.28% and 10%, for two different compatibilizers versus their (average) surface number density, σ. The data show an overall decrease of both moduli with increasing compatibilizer coverage. This decrease is more pronounced and occurs at smaller compatibilizer densities when the alkyl moieties are larger.

Notice that σ is calculated via

$$\sigma = \frac{N_A m_s/M_s}{m_f O_{CTAB}} \cdot 10^{-18}\,\text{nm}^{-2}. \quad (7)$$

Here, N_A again is Avogadro's constant, m_s/M_s is the total compatibilizer mass divided by its molecular mass. Thus, $N_A m_s/M_s$ is the total number of compatibilizer molecules in the system. The quantity m_f is the total mass of filler in the system and $O_{CTAB}=160\,\text{m}^2/\text{g}$ (cf. above). The product $m_f O_{CTAB}$ is the accessible filler surface in m^2. Calculation of σ using the above equation assumes complete reaction of compatibilizer with the accessible filler surface (notice that the size of CTAB is comparable to the size of the compatibilizer used in this study).

Already the simulated forces f_{pp} in Figure 6 indicate that the attenuation of the storage modulus in our theory do occurs at much smaller compatibilizer coverage in comparison to the experiment in Figure 7. This means that the constant c in the equation $\sigma(\text{exp})=c\ \sigma(\text{sim})$, where $\sigma(\text{exp})$ is the σ in eq. (7), is not one but must be significantly larger than one. In the following, we discuss why this is reasonable.

The experimental CTAB surface of the filler is $O_{CTAB}=160\,\text{m}^2/\text{g}$. Calculation of the total surface of a collection of isolated, smooth spheres with radius $R=15$ nm yields $87\,\text{m}^2/\text{g}$ (or $44\,\text{m}^2/\text{g}$ if $R=30$ nm). If we repeat the calculation for aggregates consisting of a large number spheres according to their volume, closely packed, of which only the outer surface is accessible, then this area is reduced by about a factor of three, that is, to roughly $30\,\text{m}^2/\text{g}$ (or $15\,\text{m}^2/\text{g}$ if $R=30$ nm). We conclude that surface roughness increases the total surface area of the experimental silica by a considerable factor. This suggests that the largest

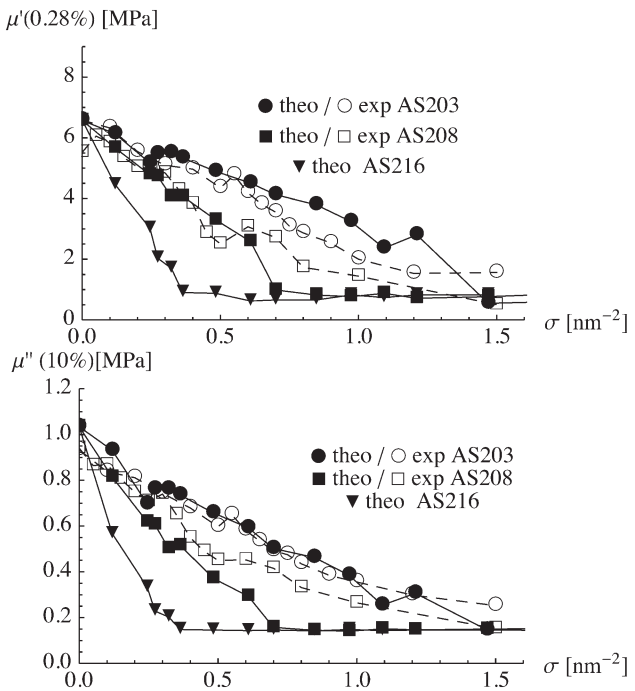

Figure 7. Storage modulus, μ', (top) and loss modulus, μ'', (bottom) versus compatibilizer surface density, σ. Open symbols: experimental data; closed symbols: theoretical results. The experimental dynamical amplitude is 0.28% in the upper panel and 10% in the bottom panel.

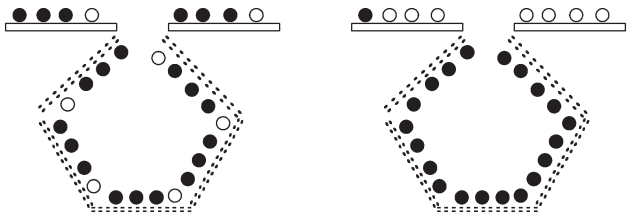

Figure 8. Illustration of homogeneous (left) versus heterogeneous (right) compatibilzer concentration. Flat solid boxes correspond to the interacting surface. Double-dashed lines correspond to the noninteracting surface, that is, the pentagon schematically represents cracks, pits, or groves on the surfaces of real filler particles. Solid circles indicate compatibilizer sites either occupied (solid circle) or empty (open circles).

portion of the filler surface consists of cracks, pits, groves, and possibly cavities, whose combined surface area, called here the noninteracting surface, does not participate in the direct interaggregate interaction considered here. Notice also that, as the simulated force curves in Figure 6 show, the important interactions do have very short range. Thus the combined surface of those cracks, pits, groves, and cavities, that is, the noninteracting surface, does not, in our model, contribute to μ' or μ''.

Because adsorption, physical and chemical, occurs preferentially at or near surface sites providing extra attractive interactions (e.g., steps, corners, pits, groves, etc.), it is not unreasonable to assume that the noninteracting surface is slightly more favored over the remaining or interacting surface. Because the interacting surface is much smaller than the noninteracting surface, even a small bias is sufficient to cause a pronounced difference in the respective surface compatibilizer densities. What we mean by bias is that the adsorption/reaction chemical potential is less on the noninteracting surface for the above energetic reason associated with its greater roughness. Figure 8 shows an illustration. The interacting surface corresponds to the flat boxes possessing compatibilizer sites indicated by circles. The double-dashed lines correspond to the noninteracting surface. The total noninteracting surface in this example exceeds the total interacting surface by a factor 5/2. The left cartoon shows the situation for a site occupation of 3/4 when all sites are equivalent. The right cartoon shows the situation when the sites on the noninteraction surface are more favorable. Their occupation has risen to 4/4, whereas the occupation on the interacting surface has diminished to 1/8. Thus, in this particular example, c has the value 8. The driving force here of course is the second law of thermodynamics. The system strives to approach the lowest possible free enthalpy. While the coverage on the interacting surface is severely reduced, the corresponding coverage change on the noninteracting surface is rather moderate. It is therefore not at all unreasonable to assume that the compatibilizer coverage on the physical surface is heterogeneous. In particular, the coverage on the interacting surface can be significantly less than the average obtained by eq. (7). Of course there also is the entropic part of the chemical potential. In particular, the mixing entropy will prevent a total depletion of the energetically less favorable surface, even if energetically more favorable empty sites on the noninteracting surface are available in excess. Based on this qualitative idea, we use c as an adjustable parameter.

Figure 7 also shows the two theoretical relations (5) and (6) in comparison to the experimental data. Throughout this comparison $c=7$. In the top panel, the storage modulus, μ', at an amplitude of 0.28% is plotted versus the compatibilizer number concentration on the surface, σ. The theoretical values are obtained via (5) using the same proportionality constant for all data points. The latter is chosen to yield agreement to within the scatter with the experimental data at vanishing compatibilizer coverage. Because the difference between μ' and $\Delta\mu'$ is small, we assume $\Delta\mu' \approx \mu'$. The bottom panel compares relation (6) to the measured loss modulus, μ'', of the same systems. The amplitude however is 10%, as explained above. Here, we have added a constant offset to all theoretical data values, accounting for the matrix contribution to the loss modules, which is not part of our model. In addition, we use $\kappa=1.3$ for the average number of opened contacts per aggregate. This number is smaller than the κ value used above. But this is perhaps not surprising, because κ should depend on the processing conditions, which differ. Overall, we obtain good correspondence between theory and experiment. It is interesting to plot the same data not versus σ but versus $\sigma^{(C*)}$, the C^*-number surface density, as shown in Figure 9. We find a significant collapse of all data onto a master curve.

To the best of our knowledge, this is the first molecular calculation of dynamic moduli of filled elastomer networks, even though a number of severe approximations are used along the way. For the latter reason, the particular value of the present calculation method, at this stage, is perhaps not its predictive power in the absolute sense. It rather offers an opportunity to compare different compatibilizers with respect to their relative effects on the dynamic moduli μ' and μ''.

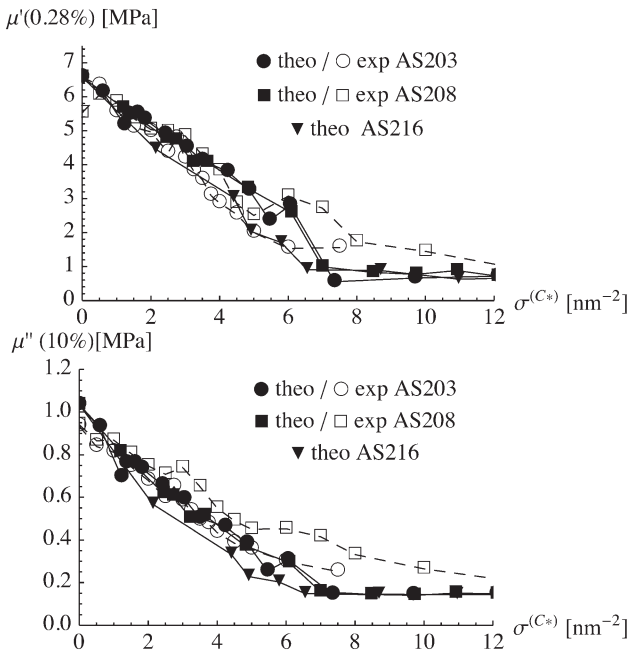

Figure 9. Experimental storage and loss moduli of Figure 7 (open symbols) together with our theoretical results (solid symbols) plotted versus the surface number density of united atom carbons, $\sigma^{(C*)}$.

DISCUSSION AND CONCLUSION

The combination of dispersion attraction between filler particles as well as other short-range attractive forces with an elastic restoring force due to the rubber matrix between the filler particles gives rise to a force loop. This in turn results in a spontaneous relative displacement of the filler particles associated with energy dissipation. This nanomechanical mechanism is akin to the jump-to-contact mechanism well known in atomic force microscopy. It is the combination of the attractive tip-to-surface interaction with the elastic cantilever force, giving rise to an analogous force loop.

The nanomechanical model presented here focuses on a single particle-particle contact. This contact is modeled in part using the MD technique based on an empirical force field. Currently, the filler material and the coupling agents are treated on a molecular level, assuming however an idealized spherical shape of the primary filler particles. The effect of the rubber matrix is included as a continuous linear elastic "collar" surrounding the contact. Despite the overall crudeness of the inclusion of molecular detail on a continuum background, which currently does not include explicit bonding between coupling agent and polymer, it appears possible to correlate the models predictions successfully with a number of experimental measurements.

Recently, other examples have been published also using force field modeling to study the interfaces and forces related to this work. Klüppel et al.[36] have investigated the rupture of filler-filler bonds in strained elastomers using MD of coarse-grained polymer chains. They find indication of a so-called glassy layer, induced into the rubber directly adjacent to the filler surface. It may be useful in this context to point out an older work by one of the authors studying the forces between helical polypeptides in solution.[37] These rodlike macromolecules do form liquid-crystalline phases in concentrated solutions. Quantitative excluded volume theories of these transitions do require the increase of the "naked" diameter of the helices, which may be interpreted in terms of "solidlike" solvent layers on the surface of the helix. A three-shell solvent layer consistent with the theories was indeed found in the above simulation study. The breaking of glassy bridges between filler particles has been studied as one of the causes for the Payne effect (e.g., Ref. 38). However, to be best of the authors knowledge no theory on this basis thus far exists, which also accounts for the pronounced effects on the Payne effect due to the molecular structure of the coupling agents. Another point requiring clarification is that the formation of a percolating (carbon black) filler network in the rubber matrix causes a pronounced drop of the materials electrical resistance.[39] It therefore is necessary to explain whether and how the concept of glassy bridges is compatible with the measured conductivity. This emphasizes that it is highly desirable to include the polymer in the above simulations and work along this line is in progress. Nevertheless, one should bear in mind that chemically realistic molecular simulations are limited to system sizes in the nm range and to the ns time scale.

Aside from the molecular modeling approach it is possible to augment our simplistic treatment of the rubber bridges between aggregates through the use of generalized Maxwell models, which would allow it to include important contributions to the overall frequency dependence left out thus far (see for instance the works of Lion and coworkers in Refs. 40 and 41 and references therein).

Before moving to the next point, we want to include one remark in this context. The authors of Ref. 42 show that the heat build up in experimental filled rubbers is reduced if the amount of sulfur in the compound (and thus the crosslink density) is increased. This is consistent with our model. We do find that W_{loss} decreases, when the matrix modulus, μ, increases (as shown in Ref. 19; notice that increasing μ also increases the slope of the matrix force in Figure 3 (bottom), which in turn reduces W_{loss}). In the same study, the heat build up also is reduced when the amount of compatibilizer is increased. Again this is consistent with the present model.

Last but certainly not least, we have taken a localized approach to the filler-filler contact by focusing on isolated contacts. Future work may show that it is necessary to include correlation effects between links, because the external strain is applied to the (fractal) strands of many aggregates.[43,44]

ACKNOWLEDGMENTS

We gratefully acknowledge the discussion of the present topic with Dr. Manfred Klüppel on the occasion of the ECCMR2013 poster session. We also want to thank the Continental Reifen Deutschland GmbH for providing the experimental data shown in the figures.

REFERENCES

1. Rauline, R. Eur. Pat. EP 0501 227, Michelin Co., **1991**.
2. Wolff, S. In The 129th Meeting of the Rubber Division American Chemical Society, New York, April 8–11, **1986**.
3. Agostini, G.; Bergh, J.; Materne, Th. Akron Rubber Group Meeting, October 27, **1994**.
4. Heinrich, G. In The Workshop Reifen of the Deutsches Institut für Kautschuktechnologie, May 25–26, **1998**.
5. Stambaugh, R. B. *Ind. Eng. Chem.* **1942**, *34*, 1358.
6. Payne, A. R. In Reinforcement of Elastomers; Kraus, G., Ed.; Wiley: New York, **1965**; Chapter 3, pp 69–123.
7. Ouyang, G. B. *Kautsch. Gummi Kunstst.* **2006**, *59*, 332.
8. Ouyang, G. B. *Kautsch. Gummi Kunstst.* **2006**, *59*, 454.
9. Vilgis, T. A.; Heinrich, G.; Klüppel, M. Reinforcement of Polymer Nano-Composites; Cambridge University Press: New York, **2009**.
10. Kraus, G., Ed. Reinforcement of Elastomers; Wiley: New York, **1965**.
11. Kraus, G. *J. Appl. Polym. Sci. Appl. Polym. Symp.* **1984**, *39*, 75.
12. Böhm, G. C. A.; Nguyen, M. N. *J. Appl. Polym. Sci.* **1995**, *55*, 1041.
13. Heinrich, G.; Klüppel, M. *Adv. Polym. Sci.* **2002**, *160*, 1.
14. Witten, T. A.; Rubinstein, M.; Colby, R. H. *J. Phys. II Fr.* **1993**, *3*, 367.
15. Huber, G.; Vilgis, T. A. *Macromolecules* **2002**, *35*, 9204.
16. Maier, P.; Göritz, D. *Kautsch. Gummi Kunstst.* **1996**, *49*, 18.

17. Sternstein, S. S.; Zhu, A.-J. *Macromolecules* **2002**, *35*, 7262.
18. Montes, H.; Lequeux, F.; Berriot, J. *Macromolecules* **2003**, *36*, 8107.
19. Hentschke, R; In Constitutive Models for Rubber VIII; Gil-Negrete, N.; Alonso, A., Eds.; CRC Press/Balkema: Leiden, **2013**; pp 299–304.
20. Böhm, J. Der Payne Effekt: Interpretation und Anwendung in Einem Neuen Materialgesetz für Elastomere, Ph.D. Thesis; Universität Regensburg: Regensburg, Germany, **2001**.
21. Gurovich, D.; Macosko, C. W.; Tirrell, M. *Rubber Chem. Technol.* **2004**, *76*, 1.
22. Marangoni, A. G.; Wesdorp, L. H. Structure and Properties of Fat Crystal Networks, 2nd ed.; CRC Press: Boca Raton, **2012**.
23. Evans, D. F.; Wennerström, H. The Colloidal Domain; VCH: New York, **1994**.
24. Payne, A. R. *J. Colloid Sci.* **1964**, *19*, 744.
25. van den Tempel, M. *J. Colloid Sci.* **1961**, *16*, 284.
26. Allen, M. P.; Tildesley, D. J. Computer Simulation of Liquids; Clarendon Press: Oxford, **1990**.
27. Burkert, U.; Allinger, N. L. Molecular Mechanics, ACS Monograph 177; American Chemical Society: Washington, D.C., **1982**.
28. Rappé, A. K.; Casewit, C. J.; Colwell, K. S.; Goddard, W. A.; Skiff, W. M., *J. Am. Chem. Soc.* **1992**, *114*, 10024.
29. Deschler, U.; Kleinschmit, P.; Panster, P. *Angew. Chem. Int. Ed. Engl.* **1986**, *25*, 236.
30. Spartan 08, Version 1.0 (MacOSX); Wavefunction, Inc.: Irvine, CA, **2008**.
31. Hojdis, N. W. Modellierung von Silica-Organosilan-Gummi-Grenzächen; Diplomarbeit, Bergische Universität: Wuppertal, Germany, **2008**.
32. Hunter, S. C. *Proc. Edinb. Math. Soc.* **1968**, *16*, 55.
33. Wrana, C. Introduction to Polymer Physics; Lanxess: Leverkusen, **2009**.
34. Baeza, G.P.; Genix, A.-C.; Degrandcourt, C.; Petitjean, L.; Gummel, J.; Couty, M.; Oberdisse, J. *Macromolecules* **2013**, *46*, 317.
35. Ziegler, J.; Schuster, R. H. *Kautsch. Gummi Kunstst.*, **2008**, *61*, 510.
36. Klüppel, M; Froltsov, V.; Juhre, D. In Constitutive Models for Rubber VIII; Gil-Negrete, N.; Alonso, A., Eds.; CRC Press/Balkema: Leiden, **2013**; pp 287–292.
37. Helfrich, J; Hentschke, R. *Macromolecules* **1995**, *28*, 3831.
38. Sotta, P.; Long, D. R.; Merabia, S.; Guy, L.; Papon, A.; Montes, H.; Lequeux, F. In Constitutive Models for Rubber VIII; Gil-Negrete, N.; Alonso, A., Eds.; CRC Press/Balkema: Leiden, **2013**; pp 315–319.
39. Niedermeier, W.; Fröhlich, J.; Luginsland, H.-D. Reinforcement Mechanism in the Rubber Matrix by Active Fillers, DEGUSSA, Technical Report 813, **2001**.
40. Lion, A.; Kardelky, C. *Int. J. Plast.* **2004**, *20*, 1313.
41. Lion, A.; Kardelky, C.; Haupt, P. *Rubber Chem. Technol.* **2003**, *76*, 533.
42. Hasse, A.; Klockmann, O.; Wehmeier, A.; Luginsland, H.-D. *Kautsch. Gummi Kunstst.* **2002**, *55*, 236.
43. M. Klüppel, private communication.
44. Xi, H.; Hentschke, R. *Eur. Polym. J.* **2012**, *48*, 1777.